PHYSICAL REVIEW D **79,** 114504 (2009)

Coulomb-gauge ghost and gluon propagators in $SU(3)$ lattice Yang-Mills theory

Y. Nakagawa,[1] A. Voigt,[2,3] E.-M. Ilgenfritz,[2,4] M. Müller-Preussker,[2] A. Nakamura,[5] T. Saito,[6] A. Sternbeck,[7] and H. Toki[1]

[1]*Research Center for Nuclear Physics, Osaka University, Ibaraki-shi, Osaka 567-0047, Japan*
[2]*Humboldt-Universität zu Berlin, Institut für Physik, D-12489 Berlin, Germany*
[3]*Max-Planck-Institut für Meteorologie, D-20146 Hamburg, Germany*
[4]*Karl-Franzens-Universität Graz, Institut für Physik, A-8010 Graz, Austria*
[5]*Research Institute for Information Science and Education, Hiroshima University, Higashi-Hiroshima 739-8521, Japan*
[6]*Integrated Information Center, Kochi University, Akebono-cho, Kochi 780-8520, Japan*
[7]*CSSM, School of Chemistry & Physics, The University of Adelaide, SA 5005, Australia*

(Received 8 March 2009; published 25 June 2009)

We study the momentum dependence of the ghost propagator and of the space and time components of the gluon propagator at equal time in pure $SU(3)$ lattice Coulomb-gauge theory carrying out a joint analysis of data collected independently at the Research Center for Nuclear Physics, Osaka and Humboldt University, Berlin. We focus on the scaling behavior of these propagators at $\beta = 5.8, \ldots, 6.2$ and apply a matching technique to relate the data for the different lattice cutoffs. Thereby, lattice artifacts are found to be rather strong for both instantaneous gluon propagators at a large momentum. As a byproduct we obtain the respective lattice scale dependences $a(\beta)$ for the transversal gluon and the ghost propagator which indeed run faster with β than two-loop running, but slightly slower than what is known from the Necco-Sommer analysis of the heavy quark potential. The abnormal $a(\beta)$ dependence as determined from the instantaneous time-time gluon propagator, D_{44}, remains a problem, though. The role of residual gauge-fixing influencing D_{44} is discussed.

DOI: 10.1103/PhysRevD.79.114504 PACS numbers: 11.15.Ha, 12.38.Gc, 12.38.Aw

I. INTRODUCTION

Lattice investigations of the gluon and ghost propagator have become an important topic over the last ten years after the pioneering lattice studies in the Landau gauge appeared in the late eighties and nineties [1–7] and after the coupled solutions to the corresponding Dyson-Schwinger equations in the deep infrared momentum region were found [8,9]. Since then, the available amount of lattice data on these propagators has grown (see, e.g., [10–21]) and also studies based on functional methods have made considerable progress [22–25] such that in Landau gauge one is nowadays in the comfortable situation to confront continuum results with a broad set of independent lattice data (see, e.g., [26–28] for recent discussions).

In Coulomb-gauge theory, comparably few lattice investigations of the aforementioned propagators have been performed. For example, Langfeld and Moyaerts [29] as well as Cucchieri and Zwanziger [30], and very recently also Burgio, Quandt, and Reinhardt [31,32] have carried out such computations for the gauge group $SU(2)$. In fact, the Coulomb gauge provides an interesting alternative to the Landau gauge since the resulting Hamiltonian approach allows one to apply the variational principle to get analytic results for the QCD vacuum wave function and for the spectrum of hadronic bound states. This approach has been mainly pursued by the Tübingen group [33] in recent years. Their investigations of (truncated) systems of Dyson-Schwinger equations in the Coulomb gauge provided various solutions in the infrared [34–36], very similar to what was found in Landau gauge and what is still under debate (see [21] and references therein).

Among us, the authors from Japan have performed several lattice Coulomb-gauge studies in the past. For the gauge group $SU(3)$, the instantaneous gluon propagators and the ghost propagator were computed in [37], and correlators of incomplete Polyakov-loops were also determined. The latter was studied in order to interpolate between the confinement potential V_c (derived from Wilson loops) and the Coulomb potential V_{Coul} (known to restrict V_c from above [38,39]). Furthermore, it was possible in this way to extract potentials for the quark-antiquark singlet and octet channels, as well as for the quark-quark symmetric sextet and antisymmetric antitriplet channels [40,41]. The eigenvalue spectrum of the Coulomb-gauge Faddeev-Popov (FP) operator was studied in [42,43].

Recently, some of us have also computed the gluon and ghost propagators as well as the Coulomb potential V_{Coul}, the latter directly from the FP operator, however [44]. For V_{Coul} very strong Gribov-copy effects were reported, and it still remains difficult to give a final answer for the infrared momentum limit [45]. Independent of that, the factorization assumption proposed in [46] relating V_{Coul} to the square of the ghost propagator was found to be strongly violated at low momenta.

In this paper we present a joint analysis of data from Humbolt University (HU), Berlin, and from the Research Center for Nuclear Physics (RCNP), Osaka, for the instantaneous propagators of both ghost and gluons. For the transverse gluon propagator as well as for the ghost propa-

gator, similar infrared properties as for the Landau gauge are expected also for the Coulomb gauge. In Landau gauge, e.g., a gluon propagator vanishing in the zero-momentum limit (or a infrared-diverging ghost dressing function) is crucial from the point of view of the Gribov-Zwanziger confinement scenario [47,48] or the Kugo-Ojima confinement criterion [49]. In the Coulomb gauge, the instantaneous time-time gluon correlator should become singular and be related to the effective Coulomb potential.

This study provides a comprehensive set of lattice data on the instantaneous gluon and ghost propagators in the Coulomb gauge of pure $SU(3)$ lattice gauge theory. We discuss their momentum dependence and analyze in detail apparent scaling violations of the space and time components of the gluon propagator. We show that these violations can be ameliorated if different cuts are applied on the data. In fact, they are effectively eliminated by a matching procedure that provides us also with the running of the lattice scale $a(\beta)$, separately for each propagator. With the exception of the time-time propagator D_{44}, we find these runnings to be in good agreement with other prescriptions. The behavior of the renormalization coefficients, that are also provided by the matching procedure, is smooth as long as $\beta \geq 6.0$.

The structure of the paper is as follows: In Sec. II we describe the setup of our lattice simulation including details on our gauge-fixing algorithms. Section III introduces the relevant lattice observables. The data for the propagators is discussed in Sec. IV where we report on obvious scaling violations for the gluon propagators. We then use a matching procedure to relate the propagators for different lattice cutoffs to each other and discuss the outcome of this for the instantaneous gluon propagators and the ghost propagator in Secs. V, VI, and VII. We present in detail the interplay of the matching procedure with the necessity of an additional momentum cutoff that restricts the reliability of the data to relatively small momenta $|pa| < \alpha$. The lattice scale dependence $a(\beta)$, as determined thereby, is compared to what is known from the literature in Sec. VIII. Finally, in Sec. IX, we discuss the momentum dependence of the propagators in both the ultraviolet and infrared region. We draw our conclusions in Sec. X. To make the paper self-consistent, we give a brief outline of the matching procedure for the Coulomb-gauge propagators in Appendix A. Fit and matching tables are presented in Appendix B.

II. LATTICE FIELD ENSEMBLES AND GAUGE-FIXING

The results discussed below are based on an extensive set of quenched gauge configurations generated in Osaka and Berlin. At both places we employed Wilson's one-plaquette action and a standard heatbath algorithm (including microcanonical steps) for thermalization, but used different values of the inverse coupling β and different lattice sizes L^4. Those, together with a couple of other useful parameters, are listed in Table I which can be found in Appendix B.

In our analysis below we combine the data from Osaka with the data obtained in Berlin. Both sets are nicely consistent with each other as we checked by comparing data at $\beta = 5.8$ and 6.0.

Configurations were fixed to the Coulomb gauge via maximizations of the Coulomb-gauge functional

$$F_U[g] = \sum_{i=1}^{3} \sum_{\vec{x},t} \frac{1}{3} \Re\mathrm{e}\,\mathrm{Tr} U_i^g(\vec{x}, t), \tag{1}$$

where $U_i^g(\vec{x}, t) = g(\vec{x}, t) U_i(\vec{x}, t) g^\dagger(\vec{x} + \hat{i}, t)$. For a fixed U this was done by iteratively changing g using a standard overrelaxation (OR) algorithm in Osaka and the simulated annealing method combined with subsequent overrelaxation (SA + OR) as in Refs. [44,45] in Berlin. Strictly speaking, different gauge-fixing methods may cause variations in the data of gauge-variant observables due to the Gribov ambiguity. This is, in particular, true for the ghost propagator at very low momentum (with deviations up to 5%, see Ref. [45] for a detailed account on that).

Each maximum of $F_U[g]$ automatically satisfies the lattice Coulomb-gauge condition

$$\nabla_i A_i^c = 0 \tag{2}$$

for all color components ($c = 1, \ldots, 8$). Here ∇_i is the lattice backward derivative in one of the three spatial directions i, and A_i^c is the lattice gluon field. Via $A_\mu = \sum_c A_\mu^c T^c$, with the eight generators T^c of $SU(3)$ in the fundamental representation, the gauge field components are defined in terms of the gauge-fixed links $U_\mu(\vec{x}, t)$ through

$$A_\mu = \frac{1}{2iag_0} [U_\mu(\vec{x}, t) - U_\mu^\dagger(\vec{x}, t)]_{\text{traceless}}, \tag{3}$$

where g_0 is the bare coupling (related to $\beta = 6/g_0^2$) and a denotes the lattice spacing. Note that we follow the midpoint definition which defines A_μ at the midpoint of a link $U_\mu(\vec{x}, t)$, i.e., $A_i \equiv A_i(\vec{x} + \frac{1}{2}\hat{i}, t)$ and $A_4 \equiv A_4(\vec{x}, t + \frac{1}{2})$.

Obviously, maximization of $F_U[g]$ proceeds independently in each time slice, as neither the Coulomb-gauge functional (1) nor the resulting gauge condition (2) fixes a link in the temporal direction. We observe that the time slices of a given configuration may behave very differently during the iterative gauge-fixing process. In fact, we find that the number of necessary iterations may differ by a factor of 10 to 20 between the individual time slices of a given configuration. This obstruction reflects that a topological tunneling might happen within one or a few subsequent time slices. In some cases there were time slices which could not be fixed within a certain predefined number of iterations. Then, the gauge-fixing process was repeated for those time slices starting from a different

randomly chosen gauge transformation g restricted to that slice, while leaving the "well-behaved" (already gauge-fixed) time slices untouched. In the majority of cases, time slices did not show any recalcitrancy during gauge fixing, though.

After all the individual time slices were maximized, the original configuration U was gauge transformed

$$U_i(\vec{x}, t) \rightarrow g(\vec{x}, t)U_i(\vec{x}, t)g^\dagger(\vec{x} + \hat{i}, t), \tag{4a}$$

$$U_4(\vec{x}, t) \rightarrow g(\vec{x}, t)U_4(\vec{x}, t)g^\dagger(\vec{x}, t + 1), \tag{4b}$$

i.e., including also the timelike links.

After having fixed the Coulomb gauge by maximizing the functional $F_U[g]$ there is still freedom to carry out gauge transformations $h_t \in SU(3)$ which only depend on time. One way to fix this residual gauge freedom is to maximize the functional

$$\tilde{F}_U[h] = \sum_t \frac{1}{3}\Re\mathrm{e}\,\mathrm{Tr}\left\{h(t)\left[\sum_{\vec{x}} U_4(\vec{x}, t)\right]h^\dagger(t + 1)\right\}, \tag{5}$$

where U is the Coulomb-gauge-transformed configuration [Eqs. (4)]. Links in time direction are finally gauge transformed under $h(t)$ as

$$U_4(\vec{x}, t) \rightarrow h(t)U_4(\vec{x}, t)h^\dagger(t + 1), \tag{6a}$$

whereas spatial links are transformed as

$$U_i(\vec{x}, t) \rightarrow h(t)U_i(\vec{x}, t)h^\dagger(t), \tag{6b}$$

which preserves the Coulomb gauge. Equal-time observables involving only spatial links, i.e., the transversal gluon or the ghost propagator, are not affected by this residual gauge freedom.

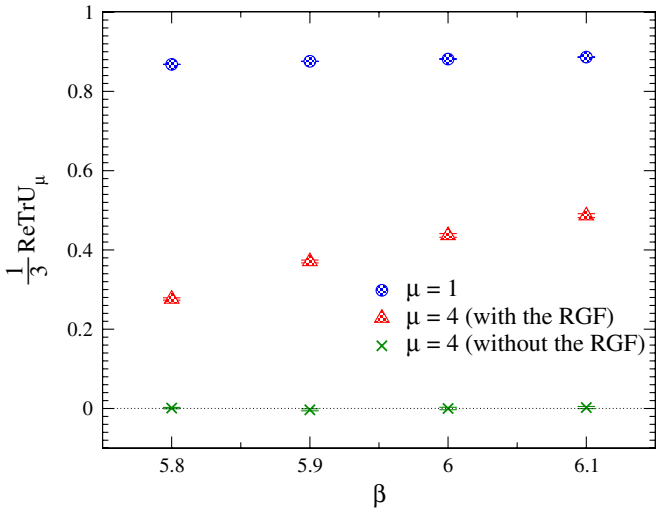

FIG. 1 (color online). Mean link values $\langle\frac{1}{3}\Re\mathrm{e}\,\mathrm{Tr}U_\mu\rangle$ for different directions μ on a 18^4 lattice. Within errors the spatial links $\langle\Re\mathrm{e}\,\mathrm{Tr}U_i\rangle$, $i = 2, 3$ (not shown) are equal to $\langle\Re\mathrm{e}\,\mathrm{Tr}U_1\rangle$. $\langle\frac{1}{3}\Re\mathrm{e}\,\mathrm{Tr}U_4\rangle$ refers to the timelike links before and after residual gauge-fixing (RGF).

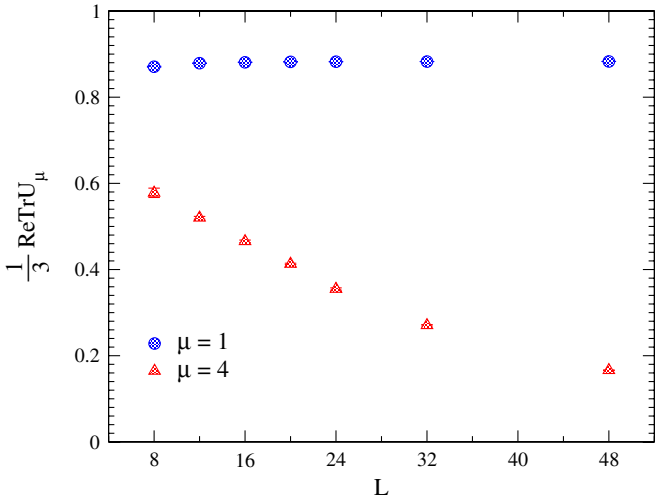

FIG. 2 (color online). Mean link values $\langle\frac{1}{3}\Re\mathrm{e}\,\mathrm{Tr}U_\mu\rangle$ for different directions μ at $\beta = 6.0$ as a function of the linear lattice size L. Notice the strong volume dependence of $\langle\frac{1}{3}\Re\mathrm{e}\,\mathrm{Tr}U_4\rangle$ after RGF.

If the transversal or the time-time gluon propagator was to be defined for non-equal time, the residual gauge would have to be fixed as well. For equal times, however, it is not clear to what extent, if at all, the results for the instantaneous time-time gluon propagator $D_{44}^{ab}(\vec{x})$ would change if the remaining gauge freedom was fixed. We will check this in Sec. VI by comparing data for D_{44} for fixed residual gauge freedom (Berlin data) to that where this freedom was left unfixed (Osaka data).

In Fig. 1 we show the average trace $\langle\frac{1}{3}\Re\mathrm{e}\,\mathrm{Tr}U_j\rangle$ for spatial links after Coulomb-gauge fixing (invariant under residual gauge fixing) and also the average $\langle\frac{1}{3}\Re\mathrm{e}\,\mathrm{Tr}U_4\rangle$ before and after residual gauge fixing as function of β. The data are taken for a 18^4 lattice. Without residual gauge-fixing the average trace of timelike links vanishes, whereas after residual gauge fixing the expectation value is finite and increases with increasing β. Figure 2 demonstrates that the average $\langle\frac{1}{3}\Re\mathrm{e}\,\mathrm{Tr}U_4\rangle$ after residual gauge-fixing (shown for $\beta = 6.0$) steeply decreases with increasing lattice volume, in contrast to $\langle\frac{1}{3}\Re\mathrm{e}\,\mathrm{Tr}U_j\rangle$ for spatial links.

In Sec. VI we will demonstrate that the difference of D_{44} measured with and without residual gauge-fixing can be completely accounted for by a multiplicative, momentum-independent rescaling, e.g., by normalizing the matched D_{44} propagator from both versions at some reference scale $p = \mu$. Apart from this, the residual gauge fixing has an impact only on the value of the propagator at zero momentum but this is not of importance for our present study.

III. COULOMB-GAUGE PROPAGATORS ON THE LATTICE

The space and time components of the gluon field evaluated in momentum space enter the bare instantaneous

transversal and time-time gluon propagator as the Monte Carlo correlators

$$D^{ab}_{ij}(\vec{k}) = \langle \tilde{A}^a_i(\vec{k})\tilde{A}^b_j(-\vec{k})\rangle, \tag{7a}$$

$$D^{ab}_{44}(\vec{k}) = \langle \tilde{A}^a_4(\vec{k})\tilde{A}^b_4(-\vec{k})\rangle. \tag{7b}$$

Here $\tilde{A}_i$ and $\tilde{A}_4$ denote the spatial Fourier transforms of the lattice gluon fields at a fixed time t with integer momenta $k_i \in (-L/2, L/2]$. An average over all time slices is understood. D^{ab}_{ij} is diagonal in color space and transverse in momentum space. On the lattice it takes the form

$$D^{ab}_{ij}(\vec{k}) = \delta^{ab}\left(\delta_{ij} - \frac{p_i(\vec{k})p_j(\vec{k})}{p^2}\right)D_{\mathrm{tr}}(p), \tag{8}$$

with

$$p_i(\vec{k}) \equiv \frac{2}{a}\sin\left(\frac{\pi k_i}{L}\right). \tag{9}$$

This is simply due to the lattice Coulomb-gauge condition which in momentum space translates into

$$\sum_{i=1}^{3} p_i(\vec{k})\tilde{A}_i(\vec{k}) = 0 \tag{10}$$

for all $\vec{k}$. In the following we use $p \equiv |\vec{p}(\vec{k})|$ to simplify the notation wherever applicable.

When analyzing data on D^{ab}_{ij} it is natural to associate the physical momentum with p. Lattice results then reproduce the continuum tensor structure of D^{ab}_{ij}. Deviations from its tree-level form are described by the dimensionless dressing function $Z_{\mathrm{tr}}(p)$, defined by

$$Z_{\mathrm{tr}} = pD_{\mathrm{tr}}(p). \tag{11}$$

Analogously, the time-time gluon propagator D^{ab}_{44} may be presented in the form of either $D_{44}(p)$ or $Z_{44}(p)$. Both are related to the full propagator through

$$D^{ab}_{44}(\vec{k}) = \delta^{ab}D_{44}(p) = \delta^{ab}\frac{Z_{44}(p)}{p}. \tag{12}$$

Depending on the particular focus, data below is presented in either one or the other form.

The ghost propagator is defined as the expectation value of the inverse FP operator M,

$$\langle (M^{-1})^{ab}_{xx'}\rangle = \delta_{tt'}\delta^{ab}G(\vec{x} - \vec{x}') \tag{13}$$

at a fixed time $t = t'$ (subsequently averaged over all time slices). The FP operator is local in time and, by virtue of the chosen Coulomb-gauge functional (1), has on the lattice the dimensionless form

$$M^{ab}_{xx'} = \delta_{tt'}\sum_{i=1}^{3}\mathrm{Re}\,\mathrm{Tr}[\{T^a, T^b\}(U_i(\vec{x}, t) + U_i(\vec{x} - \hat{i}, t))\delta_{\vec{x}\vec{x}'} - 2T^bT^aU_i(\vec{x}, t)\delta_{\vec{x}+\hat{i},\vec{x}'} - 2T^aT^bU_i(\vec{x} - \hat{i}, t)\delta_{\vec{x}-\hat{i},\vec{x}'}], \tag{14}$$

where $\hat{i}$ is a unit vector in spatial direction, $x \equiv (\vec{x}, t)$ and T^a is a generator of $SU(3)$ in the fundamental representation.

We are particularly interested in the momentum dependence of the ghost dressing function

$$J(p^2) = (\vec{p}(\vec{k}))^2G(\vec{p}(\vec{k})), \tag{15}$$

where

$$G(\vec{p}(\vec{k})) = \frac{a^2}{8L^3}\sum_{c,\vec{x},\vec{y}} e^{2\pi i\vec{k}\cdot(\vec{x}-\vec{y})/L}\langle (M^{-1})^{cc}_{\vec{x},t;\vec{y},t}\rangle. \tag{16}$$

Working in momentum space, it is convenient to invert M for a selection of momenta and colors c forming right-hand side plane-wave sources $\xi^c(k) = \delta^{ac}e^{2\pi ik\cdot x/L}$ with $k = (\vec{k}, 0) \neq 0$. We use a preconditioned conjugate-gradient algorithm described in Ref. [13], adapted to the Coulomb gauge, to accelerate the inversion of M. Alternatively, we could have used a selection of point sources ξ and Fourier transformed the vectors $[M^{-1}\xi](x)$ providing an estimator for the ghost propagator at once for all momenta, however with less statistical accuracy. The plane-wave method automatically ensures that $J(p^2)$ is averaged over all time slices. Moreover, translational invariance is exploited to improve the estimator. Note that M cannot be inverted for $\vec{k} = 0$ due to its eight trivial (constant) zero eigenmodes.

Multiplicative renormalizability is a well established property of the gluon and ghost propagators in the Landau gauge. In the Coulomb gauge, to our knowledge, this has been proven yet only up to one loop by Watson and Reinhardt quite recently [50]. Their result for the bare dressing functions obtained in the 4D momentum space, formally translated from dimensional to lattice regularization looks as follows (omitting possible lattice corrections):

$$\begin{aligned} Z^L_{\mathrm{tr}} &= 1 + g_0^2C_{\mathrm{tr}}[\log(a^2(x+y)) + H_{\mathrm{tr}}(\zeta)] + O(g_0^4),\\ Z^L_{44} &= 1 + g_0^2C_{44}[\log(a^2(x+y)) + H_{44}(\zeta)] + O(g_0^4),\\ J^L &= 1 + g_0^2C_J[\log(a^2y) + H_J] + O(g_0^4), \end{aligned} \tag{17}$$

where the momentum variables are $x = p_4^2$, $y = \vec{p}^2$, $\zeta = x/y$, and the lattice cutoff is a^{-1}. C_{tr}, C_{44}, C_J, and H_J denote constants. Note the nontrivial dependence on ζ for both the Coulomb-gauge gluon dressing functions. When multiplicatively renormalizing the dressing functions, e.g., in a momentum subtraction scheme at some scale μ, this dependence has to be carefully taken into account (see also [32]), in particular, for equal-time correlators which according to Eq. (17) require an integration over p_4 or ζ. Of

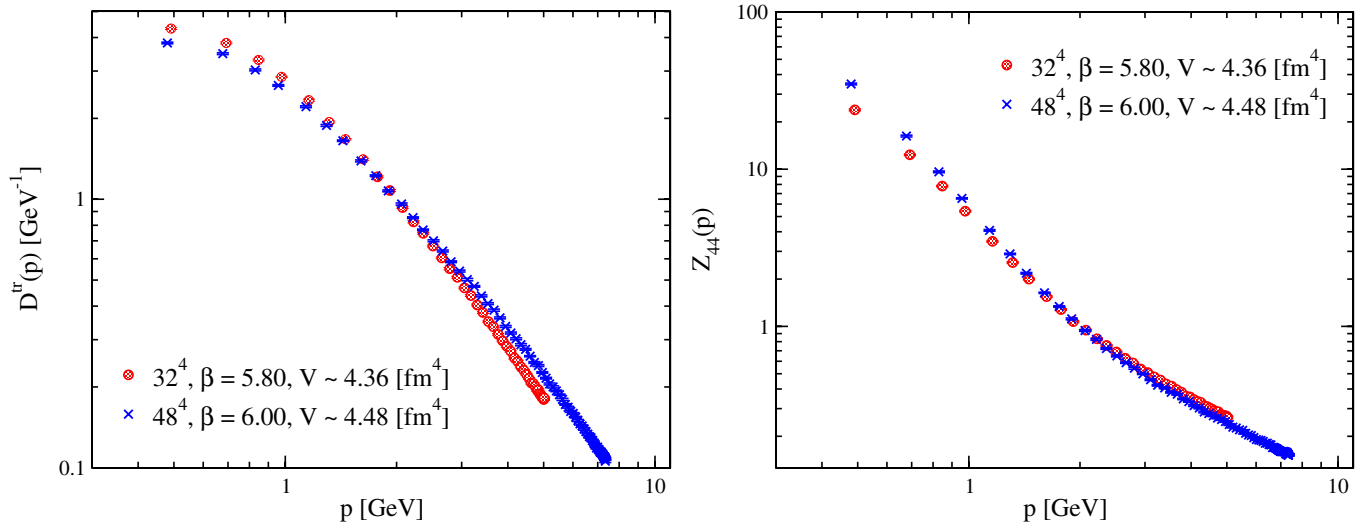

FIG. 3 (color online). The instantaneous transverse gluon propagator (left) and the dressing function of the instantaneous time-time gluon propagator (right) using the Necco-Sommer scaling relation and normalized at $\mu = 2$ GeV. The data refers to approximately equal physical volumes and has been cylinder and cone cut. Data was produced at HU, Berlin.

course, $a^{-1} \gg \mu$ has to be ensured for that which, admittedly, is very difficult to achieve in nowadays lattice computations. Even more, lattice computations are typically carried out at several values of β, i.e., at different cutoff values. In general one should expect that the corresponding dressing functions at different lattice spacings, say a and $\bar{a}$, are related to each other by a finite renormalization of the Z factors which will obviously depend only on the ratio $\bar{a}/a$ and not on the momenta. This will then hold also for the dressing functions Eq. (17) and correspondingly also for the equal-time correlators.

In the case of the Landau gauge those Z factors turned out to be close to unity for the gluon and ghost dressing functions at similar values of β. Therefore, it is more or less sufficient for them to express the various lattice spacings by a unique physical scale, e.g., via the Sommer-scale parameter $r_0 = 0.5$ fm and the interpolation formula of Necco and Sommer [51]

$$\ln(a/r_0) = -1.6804 - 1.7331(\beta - 6.0) + 0.7849(\beta - 6.0)^2 - 0.4428(\beta - 6.0)^3 \quad (18)$$

obtained from the lattice analysis of the static quark-antiquark potential and applicable in the range $5.7 \leq \beta \leq 6.92$. The remaining lattice artifacts were sufficiently dealt with by applying cone and cylinder cuts to the momenta [52]. While a cone cut addresses finite-volume effects, the cylinder cut is an easy and effective method to reduce artifacts due to the broken rotational symmetry. We shall apply both these cuts also to our data shown below. However, in what follows we will demonstrate that the approach, even if sufficient for the Landau gauge, is not quite enough for the case of the Coulomb gauge. In fact, besides applying the usual cone and cylinder cuts one has to restrict momentum components to also satisfy $ap_i \leq \alpha < 2$ and to apply nontrivial finite renormalizations between the different cutoff values.

Also, we shall not use *a priori* the Necco-Sommer scaling relation [Eq. (18)] but instead find the specific scaling behavior for each of the propagators defined above and present their data in terms of the finest available lattice scale at either $\beta = 6.20$ or 6.10. For this we employ the matching procedure of Ref. [52] adapted here to the Coulomb gauge. A detailed outline of this method applied to our propagators is given in Appendix A.

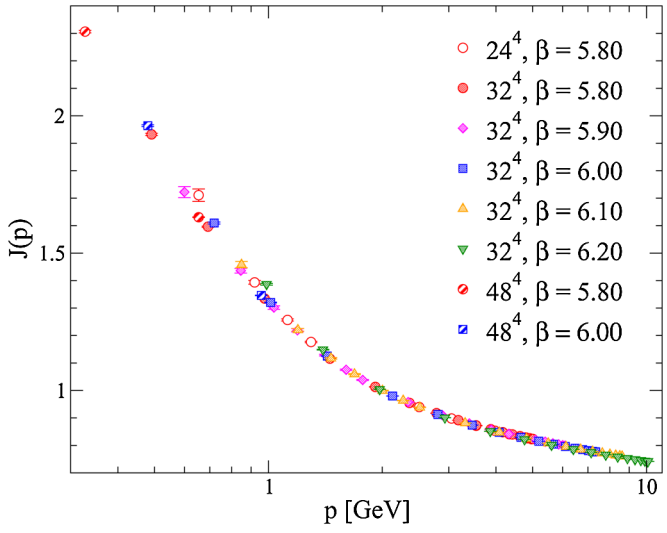

FIG. 4 (color online). The ghost dressing function using the Necco-Sommer scaling relation and normalized at $\mu = 2$ GeV. The data has been cylinder and cone cut. Data at $\beta = 5.8$, 6.0, 6.2 was collected at HU, Berlin, data at $\beta = 5.9$, 6.1 at RCNP, Osaka.

IV. DISCRETIZATION ERRORS OF THE BARE LATTICE DATA

We start our discussion by revisiting the strong scaling violations we reported for the transversal and the time-time gluon propagator in [37,44]. There, we used the interpolation formula equation (18) to assign physical units to the lattice momenta and applied a multiplicative normalization at $\mu = 2$ GeV for all values of β. This procedure, however, leads to serious disretization errors for both the instantaneous transversal and the time-time gluon propagator (see Fig. 3), whereas the ghost propagator looks much more satisfactory in this respect (see Fig. 4).

Challenged by these scaling violations, in the next sections we shall perform a matching procedure that merges the data for different β into one bare lattice propagator associated with the highest available lattice cutoff.

In a first step, however, we consider here the scaling violations. We argue that they indicate that the admissible range of lattice momenta needs to be restricted even further than what the cylinder and cone cut would do. For this, we introduce a new momentum cut that will be applied in addition to those two cuts. Basically, the full Brillouin zone should not be eligible when analyzing the corresponding propagator data, but only that at momenta [Eq. (9)] whose components are restricted to $|p_i a| \leq \alpha < 2$. For the sake of brevity we will refer to this cut as the "α cut" in what follows.

Figure 5 illustrates the effect of the α cut on the instantaneous transversal gluon propagator. Note that in this figure (as in [37,44]) we have used the Necco-Sommer formula (18) (and $r_0 = 0.5$ fm) to assign physical units to momenta and propagator. Obviously, when decreasing α less and less data points survive this cut but those that do

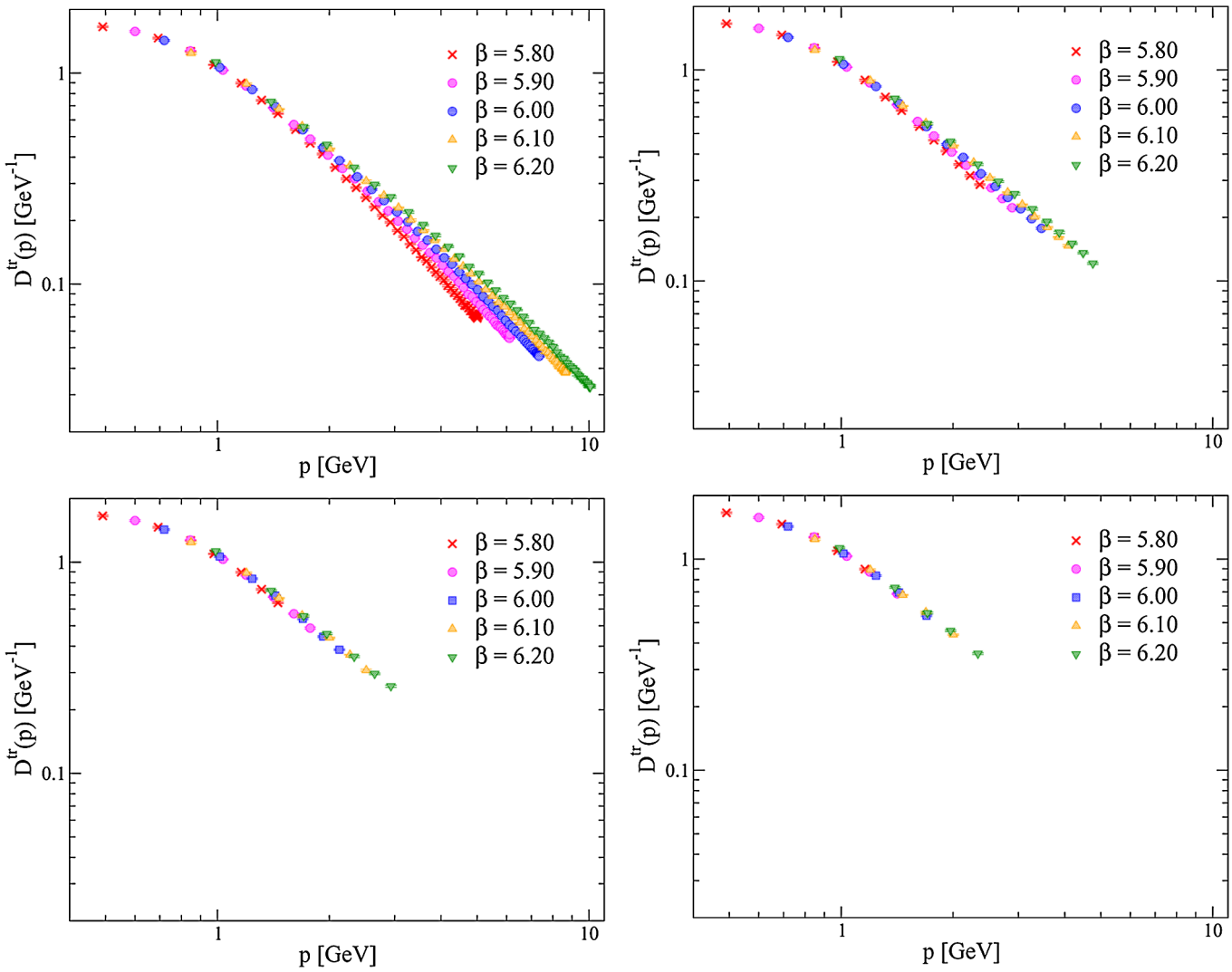

FIG. 5 (color online). Effect of the α cut on the bare lattice data of the instantaneous transverse gluon propagator. The data (all for a 32^4 lattice) is presented imposing different α cuts: no α-cut (top left), $|p_i a| \leq 1$ (top right), $|p_i a| \leq 0.6$ (bottom left), $|p_i a| \leq 0.5$ (bottom right). Cylinder and cone cuts have been applied as before. Necco-Sommer scaling (with $r_0 = 0.5$ fm) has been used to get $a(\beta)$ and physical momenta p. The data for $\beta = 5.8$, 6.0, 6.2 (5.9, 6.1) was obtained at HU, Berlin (RCNP, Osaka).

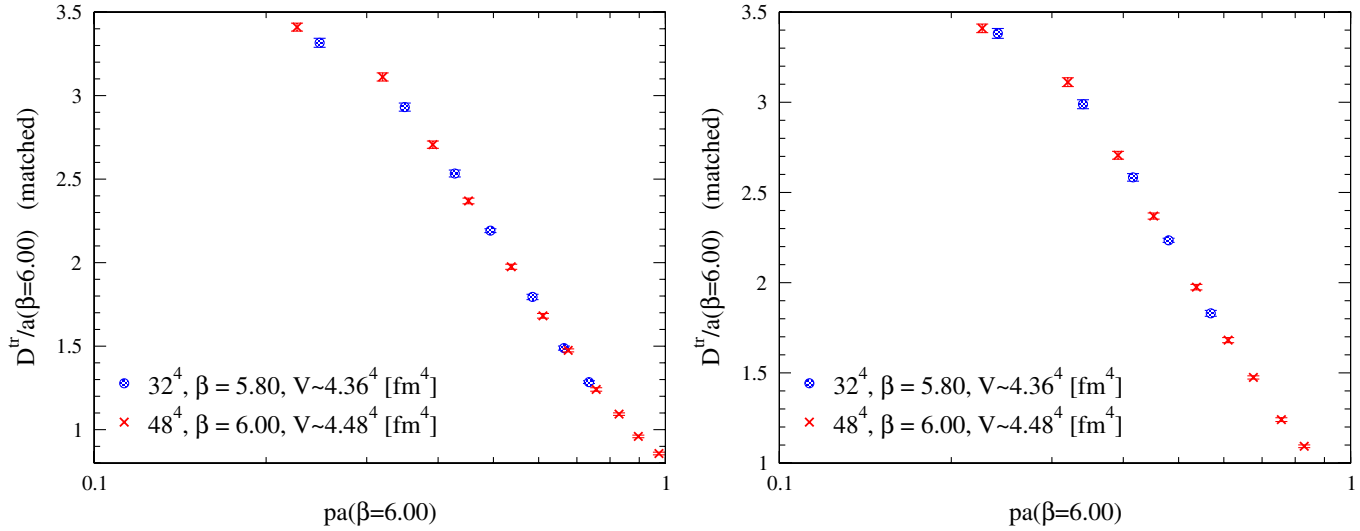

FIG. 6 (color online). The instantaneous transverse gluon propagator obtained by matching data from two lattices with approximately equal physical volume. Besides cylinder and cone cuts, an α cut has been imposed with $\alpha = |p_i a| \leq 0.6$ (left) and $\alpha = |p_i a| \leq 0.5$ (right). Data collected at HU, Berlin.

show a much better overlap than before (see, in particular, the lower panels of Fig. 5).

V. MATCHING THE TRANSVERSAL GLUON PROPAGATOR

Still, the disagreement between data from different β does not completely disappear. Therefore, in a next step, we relax the *a priori* universal $a(\beta)$ dependence [e.g., that according to Eq. (18)] and apply the matching procedure of Ref. [52] as explained in Appendix A. It provides us with multiplicative renormalization factors depending on the ratios of the lattice spacings and with the specific dependence of the lattice spacing $a = a(\beta)$ separately for each propagator.

We start with the instantaneous transversal gluon propagator and first match data obtained on two lattices with approximately the same physical volume, i.e., data on a $L^4 = 32^4$, $\beta = 5.8$ lattice with data on a $L^4 = 48^4$, $\beta = 6.0$ lattice. Besides the cone and cylinder cuts we apply two different α cuts (with $\alpha = 0.6$ and $\alpha = 0.5$) before performing the matching procedure. Our aim is to compare the influence of the α cut on the quality of matching. The result, with $L^4 = 32^4$, $\beta = 5.8$ being the coarse and $L^4 = 48^4$, $\beta = 6.0$ being the fine lattice, is shown in Fig. 6 for both α cuts.

We obtain good matching of both data sets with a better result for $\alpha = 0.5$ (see the χ^2/dof listed in Table II). There is hardly any difference between the best result of the matching procedure on the one hand and directly imposing the Necco-Sommer scaling relation on the other (Fig. 5). Indeed, our matching procedure nearly reproduces the lattice-spacing ratios as given through Eq. (18) (see Table II in Appendix B).

Next we extend the matching to *all* values of $\beta = 5.8 \ldots 6.2$ using data obtained on 32^4 and 48^4 lattices. Since $\beta = 6.2$ has the finest lattice spacing, the matching is performed between data at $\beta = 6.2$ (setting the reference scale) and data at all other $\beta = 5.8 \ldots 6.1$. We also compare the result for four different α cuts. The results are summarized in Table III.

We not only find the ratios of lattice spacings to rise monotonously upon decreasing β, but also the ratios of the renormalization constants to be about the same (somewhat below 1.0), i.e., almost independent on β.

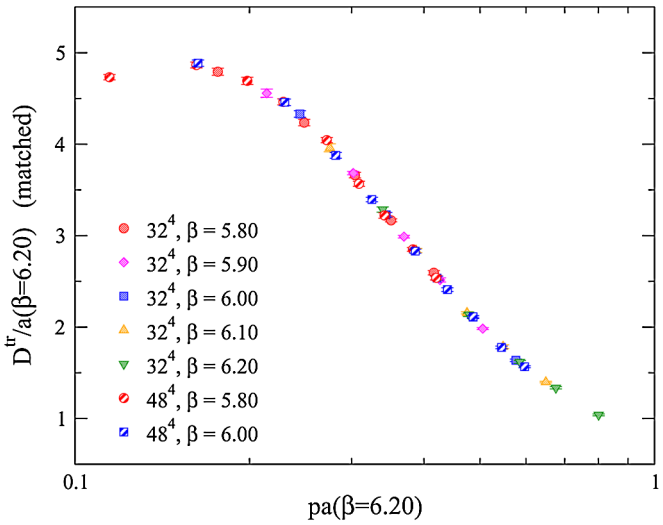

FIG. 7 (color online). The instantaneous transverse gluon propagator obtained by matching all data from 32^4 and 48^4 lattices, including data from both Osaka and Berlin collected at five different β values. The result is shown for a fixed α cut with $|p_i a| \leq 0.5$. Data are cylinder and cone cut.

As a general rule, smaller values for α result in lower χ^2/dof values and hence better matching. We also see that the matching procedure nearly always results in a lattice-spacing ratio smaller than that given through Eq. (18), although the discrepancy decreases with α taken smaller. As shown in Fig. 7 for the best α cut ($\alpha = 0.5$), we achieve a virtually perfect matching of the instantaneous transversal gluon propagator over all data obtained at $\beta = 5.8 \ldots 6.2$. Comparing with the χ^2/dof for $\alpha = 1.0$, we conclude that applying the α cut is essential to achieve a good overlap of the data. Our combined final result indicates a flattening of the propagator in the infrared region which is worth to be explored further. We expect a tendency to show a plateau as recently seen in the Landau gauge case [21], which excludes a vanishing gluon propagator in the infrared limit.

VI. MATCHING THE TIME-TIME GLUON PROPAGATOR

We now apply the matching procedure to the instantaneous time-time gluon propagator D_{44}. As for the transversal propagator D_{tr}, we first match data obtained on two lattices with approximately the same physical volume, i.e., data for $L^4 = 32^4$, $\beta = 5.8$ with data for $L^4 = 48^4$, and $\beta = 6.0$, respectively. We also compare the effect of two different α cuts ($\alpha = 0.6$ and $\alpha = 0.5$) in addition to the usual cylinder and cone cuts.

Whereas the matching seems to work reliably as shown in Fig. 8 and as demonstrated in Table IV by the low χ^2/dof value for $\alpha = 0.5$, the obtained lattice-spacing ratio is now significantly larger than predicted by the Necco-Sommer scaling relation (see Table IV). This is in striking contrast to what we have observed in the case of the transversal gluon propagator.

We now merge *all* data for D_{44} in the interval $\beta = 5.8 \ldots 6.2$ obtained on the 32^4 and 48^4 lattices. However, since the instantaneous time-time gluon propagator is more sensitive to Gribov copies [44] and since we have employed different gauge-fixing procedures at Berlin and Osaka: we first match the corresponding data sets separately. The resulting fit parameters are summarized in Table V (Osaka) and Table VI (Berlin).

Matching the Osaka data one finds that the ratios R_a of lattice spacings rise monotonously upon decreasing β but much stronger than in Eq. (18). The ratio of renormalization constants is still compatible with unity for $\beta = 6.0$ if compared to $\beta = 6.1$ (providing the reference scale), but it decreases abruptly between $\beta = 6.0$ and $\beta = 5.9$. The χ^2/dof value is acceptable only for an α cut where $\alpha = 0.5$.

The Berlin data allows one to compare only $\beta = 6.0$ and $\beta = 5.8$ to $\beta = 6.2$ (which sets the reference scale). The ratios of the lattice spacings are compatible with the results for the Osaka data. The ratio of the renormalization constants is still compatible with unity for $\beta = 6.0$, if compared to $\beta = 6.2$, but drops between $\beta = 6.0$ and $\beta = 5.8$, similar to the Osaka data. The χ^2/dof is unacceptably large.

In Fig. 9 we show our final result for the instantaneous time-time gluon propagator having matched and combined all the Osaka and Berlin data. We have now used a unique scale set by $a(\beta = 6.0)$ to give all momenta in physical units. The quality of the fits in this case is worse compared with the fits of the transverse gluon propagator. Nevertheless, the scaling behavior does look quite reason-

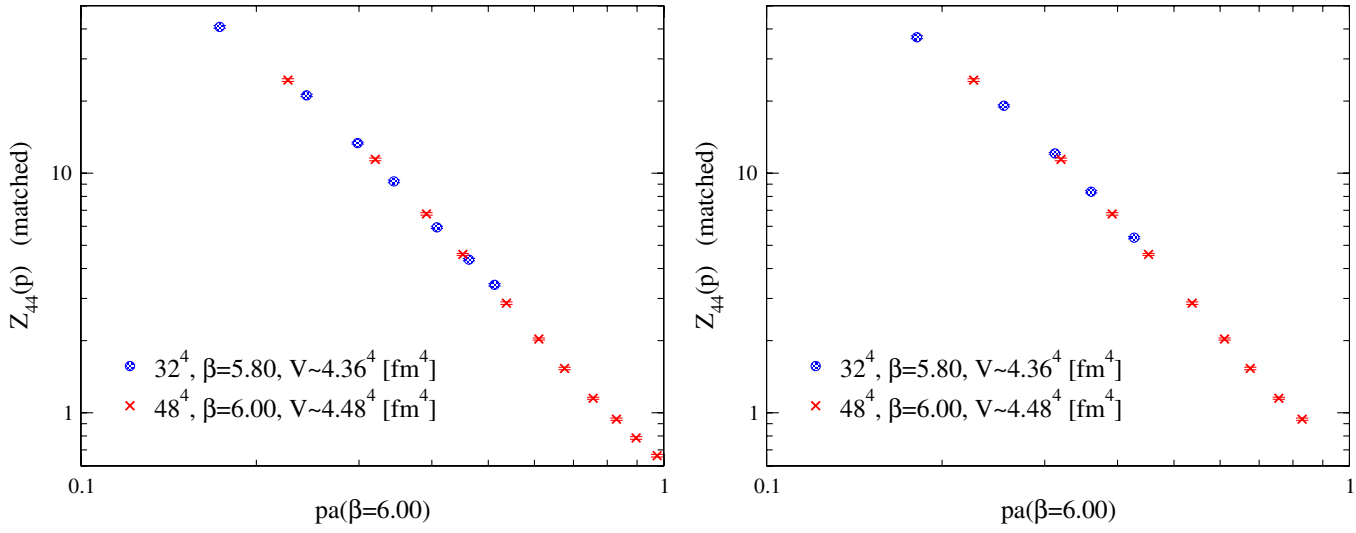

FIG. 8 (color online). The instantaneous time-time gluon dressing function after matching Berlin data from two lattices of approximately equal physical volume and applying cylinder and cone cuts. Two α cuts are compared: $|p_i a| \leq 0.6$ (left) and $|p_i a| \leq 0.5$ (right).

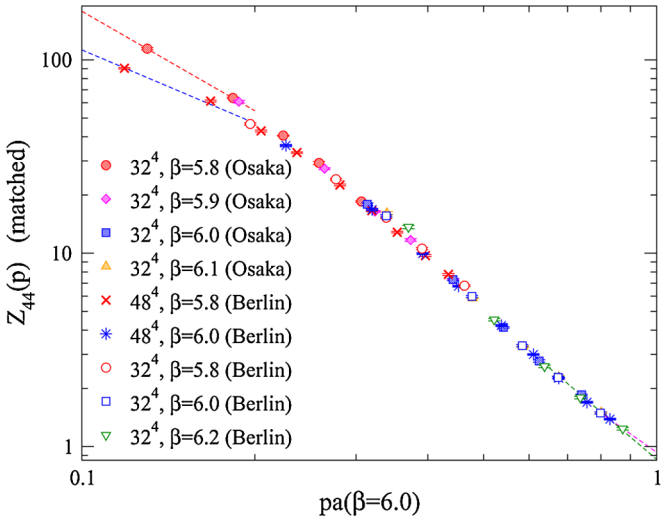

FIG. 9 (color online). The dressing function of the instantaneous time-time gluon propagator after matching Berlin and Osaka data separately on 32^4 and 48^4 lattices for five different β values. The fit parameters emerging from the matching are listed in Tables V and VI. Data has been cylinder and cone cut and results are shown for a fixed α cut with $|p_i a| \leq 0.5$. The two fits for the momentum dependence in the IR are described in Sec. IX.

able and there is an improvement compared to the results presented in Table IV. The reason is probably that we have moved closer to the continuum limit by including data from $\beta = 6.1$ and $\beta = 6.2$. In the infrared region the data points obtained in Berlin and Osaka split. We interpret this as a consequence of the use of different gauge-fixing techniques. The more efficient simulated annealing method weakens the singular behavior as seen also for the ghost propagator [45].

In passing, we revisit the question of whether there is a difference between the instantaneous time-time gluon propagator if one is applying the residual gauge-fixing (Berlin data) or not (Osaka data). Figure 10 shows the results for $\beta = 6.0$. The propagator at momentum $pa \neq 0$ seems not to depend on the volume, but on the procedure (cf. the left panel). The latter is understandable if one looks back at Fig. 1 and there at the difference for the timelike links. It is remarkable that the difference between the two cases can be eliminated by a uniform multiplicative rescaling. This is accomplished by normalizing the propagator D_{44}/a at $pa = 2.0$ to 1.0 (cf. the right panel). The residual gauge fixing has only an impact on the value of the propagator at zero momentum, $D_{44}(ap = 0)/a$. With residual gauge fixing this value is obviously smaller as expected.

VII. MATCHING THE GHOST PROPAGATOR

Finally we apply the matching procedure to the ghost propagator. As we have seen in Fig. 4, Necco-Sommer scaling is only weakly violated. Therefore, we expect a matching result that closely follows this behavior.

The fitting results (respectively for the Osaka and Berlin data) are presented in Tables VII and VIII, there relative to the highest $\beta_{\max} = 6.1$ and $\beta_{\max} = 6.2$ in both cases. For no α cut ($\alpha = 2.0$) the ratios of lattice spacing $a(\beta)/a(\beta_{\max})$ reproduce almost perfectly the corresponding ratios according to Eq. (18). Nevertheless, we notice that a smaller α leads to some deviation from that scaling, in particular, at the lowest β. Including the results of the separate fits, the Osaka and Berlin data are afterward combined in Fig. 11 showing there the result only for the most restrictive α cut ($\alpha = 0.5$).

Matching the Osaka data yields an overall very good χ^2/dof. The ratios of the renormalization constants are all

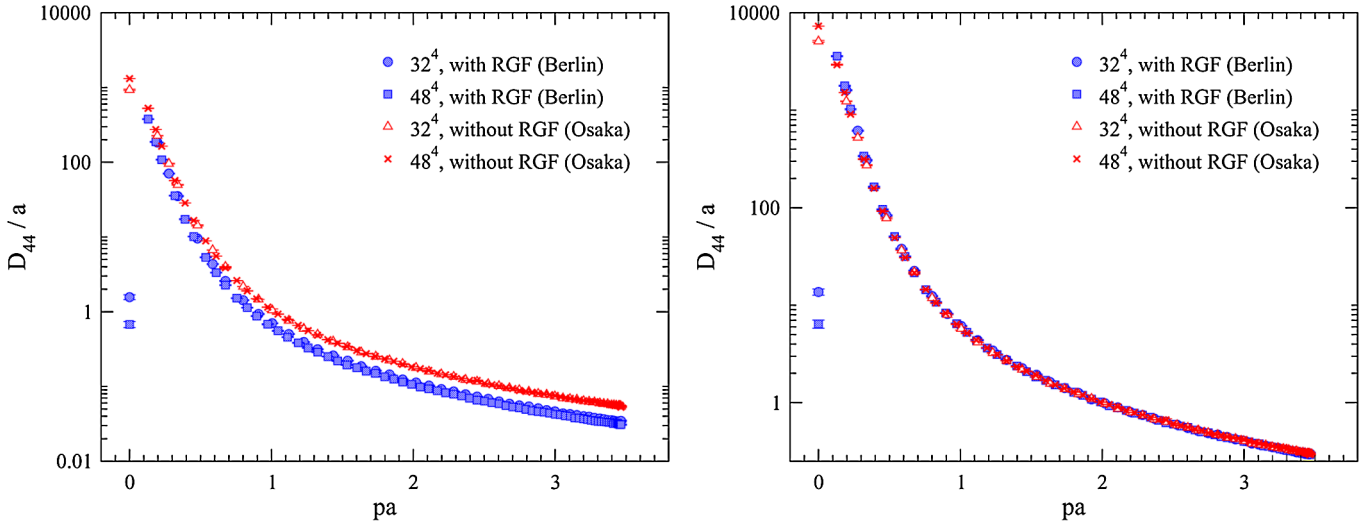

FIG. 10 (color online). Left: comparison between the unrenormalized instantaneous time-time gluon propagator D_{44} with and without the residual gauge fixing. Right: the same but formally normalized at $pa = 2$. The cylinder cut has applied to all data. Berlin and Osaka data for $\beta = 6.0$ and lattice sizes 32^4 and 48^4 are shown together.

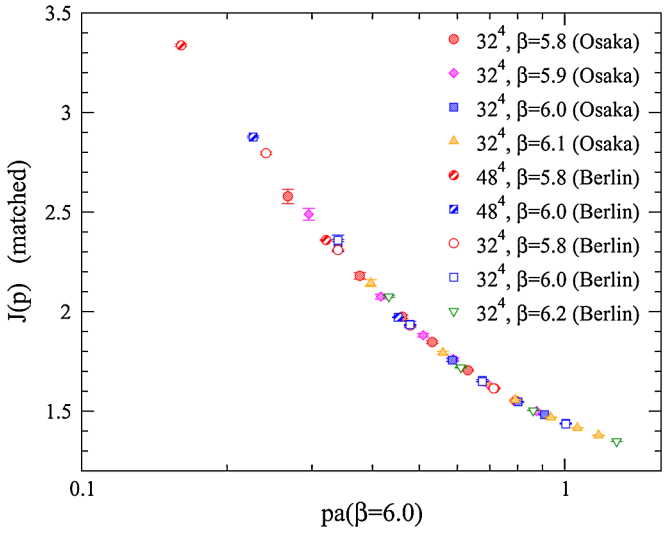

FIG. 11 (color online). The ghost dressing function after matching data from the 32^4 and 48^4 lattices including data from both Osaka and Berlin at five different β values. For the fits see Tables VII and VIII. The result is shown for a fixed α cut: $|p_i a| \leq 0.6$. Both the cylinder and the cone cut are applied as usual.

compatible with unity, and the ratios of lattice spacings rise monotonously upon decreasing β. When no α cut is applied the fitted R_a rise in accordance with Eq. (18), while restricted α cuts lead to R_a's which grow slightly slower. Matching the Berlin data results in the same tendencies, but the χ^2/dof turned out to be very large. This is probably due to the fact that the Berlin ghost data are averaged over all time slices and the Osaka data are not; the errors of the Berlin data are smaller by an order of magnitude.

VIII. THE SCALING BEHAVIOR OF THE PROPAGATORS

At this point we can check now if our individual results on $a(\beta)$ reproduce a unique running lattice scale. We had started with Necco-Sommer scaling, but abandoned this, fully relying on the matching procedure to produce the "correct" lattice scale function. Let us remember that the lattice scales as found may deviate from asymptotic scaling (which of course is strictly valid only for $\beta \to \infty$) and also from that derived for other observables (e.g., Necco-Sommer scaling derived for the static quark-antiquark force in pure $SU(3)$ gauge theory).

With Fig. 12 we summarize our results on the fitted scaling behavior of the lattice spacing in terms of the finest lattice spacing available in our study. For all the propagators considered we have plotted the ratios of the lattice spacings relative to the finest lattice (at $\beta = 6.2$ for the transverse gluon propagator in the left panel, and at $\beta = 6.1$ for D_{44} and the ghost propagators in the right panel, respectively) as a function of β as found through the matching procedure with two choices of the α cut. For the transversal gluon propagator the data points (corresponding to both choices of α cuts) fit very well between the curves corresponding to the two-loop running of the lattice spacing

$$a = \frac{1}{\Lambda_{\mathrm{Lat}}}\left(\frac{8\pi^2}{11N_c}\beta\right)^{51/121}\exp\left(-\frac{4\pi^2}{11N_c}\beta\right), \qquad (19)$$

and to the relation [Eq. (18)]. The same is observed for the ghost propagator. In this case, also applying no cut ($\alpha = 2.0$) results in a reasonable result.

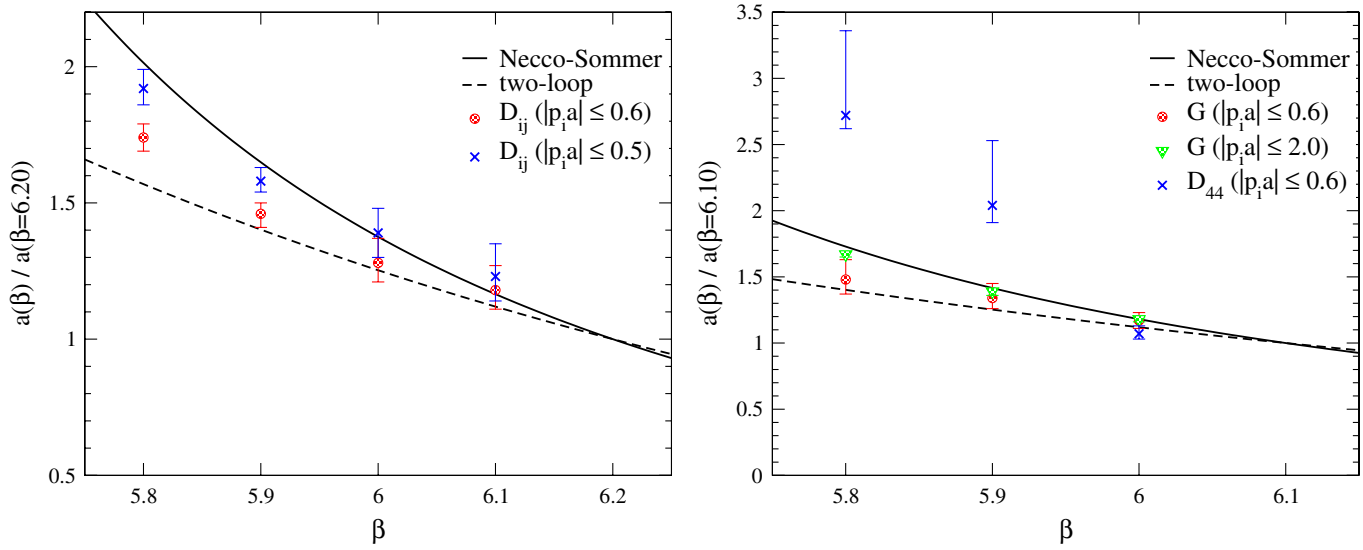

FIG. 12 (color online). The scaling relation as it emerges from matching the data obtained in simulations with the Wilson action. Left: the running lattice scale extracted from the transversal gluon propagator (with two α cuts for comparison). Right: the running lattice scale extracted from the ghost propagator (with no α cut, i.e. $\alpha = 2.0$, and with an $\alpha = 0.6$ for comparison) together with the running lattice scale obtained from the time-time gluon propagator (with a rather conservative cut at $\alpha = 0.6$).

On the other hand, the $a(\beta)$ dependence as found from the matching procedure of the instantaneous time-time gluon propagator is not only much stronger than in Eq. (18), but also inconsistent with the scaling law for the other propagators. We cannot say to which extent such a faster running is beyond some general bound and unfortunately have to conclude that the problem of the bad scaling behavior for the instantaneous time-time gluon propagator remains unsolved yet.

IX. FITTING THE BEHAVIOR AT LARGE AND SMALL MOMENTUM

Having successfully merged data for the propagators from simulations at different β values, one may try to fit their ultraviolet (UV) behavior and partly also to extract some infrared (IR) exponents.

For the transverse gluon propagator we try a power-law ansatz

$$D^{\mathrm{tr}}(|\vec{p}|)^{\mathrm{UV}} = \frac{1}{|\vec{p}|}\left(\frac{c_{\mathrm{tr}}}{|\vec{p}|}\right)^{\eta_{\mathrm{tr}}}, \tag{20}$$

to describe the behavior at large momenta. For the UV fitting we use the data points above some minimal momentum $[|\vec{p}|_{\mathrm{min}}$ in units of $a^{-1}(\beta = 6.2)]$ and investigate the dependence of the anomalous dimension η_{tr} on the fitting range and the α cut. Fit results are collected in Table IX and our best fits (with $\alpha = 0.5$) give $\eta_{\mathrm{tr}} = 0.40(2)$. Qualitatively, the behavior we find is similar to the UV fit given in Ref. [29], though there [for $SU(2)$] a somewhat bigger exponent $\eta_{\mathrm{tr}} = 0.5(1)$ was found.

For the longitudinal gluon dressing function Z_{44} we try power-law ansatzes both in the UV and in the IR regions

$$Z_{44}(|\vec{p}|)^{\mathrm{UV}} = \left(\frac{c_{44}}{|\vec{p}|}\right)^{\eta_{44}}, \qquad Z_{44}(|\vec{p}|)^{\mathrm{IR}} = \left(\frac{d_{44}}{|\vec{p}|}\right)^{\kappa_{44}}. \tag{21}$$

The results are collected in Tables X and XI, respectively. This dressing function was not studied in Ref. [29].

For the ghost dressing function, analogous to Ref. [29], we adopt a logarithmic ansatz in the UV region

$$J(|\vec{p}|)^{\mathrm{UV}} = \frac{c_{\mathrm{gh}}}{\ln(|\vec{p}|/\Lambda_{\mathrm{Coul}})^{\gamma}}, \tag{22}$$

and a power-law ansatz for the IR behavior

$$J(|\vec{p}|)^{\mathrm{IR}} = \left(\frac{d_{\mathrm{gh}}}{|\vec{p}|}\right)^{\kappa_{\mathrm{gh}}}. \tag{23}$$

Fits results for either momentum region are given in Tables XII and XIII, respectively. The UV fits scatter with α (the additional momentum cut), though, the most stable results are obtained for no α cut ($\alpha = 2.0$). With a suitably restricted fit interval fits are stable and give $\Lambda_{\mathrm{Coul}}a(\beta = 6.0) = 0.275(20)$ or $\Lambda_{\mathrm{Coul}}r_0 = 1.37(10)$ and $\gamma = 0.33(1)$. For $SU(2)$ this exponent was found to be $\gamma = 0.26(2)$ [29].

The IR fits are quite stable and give $\kappa_{\mathrm{gh}} = 0.435(6)$ without applying α cuts, even though we admit that the χ^2/dof values are rather large. In Ref. [29] a value $\kappa_{\mathrm{gh}} = 0.49(1)$ was found (corresponding to 2κ there).

X. CONCLUSIONS

We have investigated the momentum dependence of the instantaneous ghost and gluon propagators of pure $SU(3)$ lattice Coulomb-gauge theory. Our study represents a joint analysis of data from lattice simulations independently performed at Berlin and Osaka for the Wilson gauge action in the range $\beta = 5.8, \ldots, 6.2$.

For these values of β, we find apparent scaling violations for both the spatially transversal and the time-time gluon propagator, while for the ghost propagator such violations are surprisingly mild. Our inspection of the gluon propagator data shows that the violations there are basically due to data that survives a cylinder cut but involves momentum components close to the upper end of the Brillouin zone. Consequently, if additionally an α cut like $|p_i a| \leq 0.5$ is applied to the data, scaling violations are under much better control. The price to pay is strong restrictions of allowed momenta which, in our opinion, should not only satisfy the cylinder and cone cuts but also $|p_i a| \leq 0.5$ (α cut). This is the first result of our paper. Note that an alternative method for handling (hypercubic) lattice artifacts is proposed in Refs. [6,53,54]. This could allow for less restrictive cuts on the data and is left for a future study.[1]

Second, we find that the scaling violations can be sufficiently reduced if, in addition to the aforementioned cuts, a matching procedure (see Appendix A) is used to merge data. That is, instead of imposing one particular $a(\beta)$ dependence (e.g., that of Ref. [51]) and normalizing the data for the different lattice cutoffs such that they coincide at a particular reference scale, both the $a(\beta)$ dependence and the relative normalization factors are determined through an optimization method that seeks the best overlap of data. It turns out that the matching procedure applied to either the transversal gluon or the ghost propagator provides us with a $a(\beta)$ dependence only slightly different from what is known from [51], somewhere in between Necco-Sommer scaling and asymptotic two-loop scaling. Note that the matching procedure would allow us to fix the lattice spacing if we were to simulate also beyond the interval $5.7 \leq \beta \leq 6.92$ covered by the Necco-Sommer analysis. In any case, our approach of relating all the data for the different β values to the highest available lattice cutoff, i.e., to the smallest lattice spacing, cannot completely remove the cutoff dependence. Though, this should become weaker upon increasing β.

Generally we can say that the matching analysis results in ratios of the renormalization constants closer to unity at $\beta \geq 6.0$. Future lattice studies of gluon and ghost propa-

[1]We gratefully acknowledge useful comments from the referee.

gators should be performed in that region. The fact that—except for the ghost propagator—the matching performs better when the more restrictive α cuts are applied shows that the momenta with components close to the upper end of the Brillouin zone are far from the continuum limit. This might signal a more general effect, namely, that observables closer to the infrared region have better scaling properties.

Unfortunately, we could not correct the scaling violations for the instantaneous time-time gluon propagator. For this, these violations are so strong that the $a(\beta)$ dependence as found through the matching is far from what we find for the other propagators. In fact, $a(\beta)$ in this case is found running too fast. Moreover, for $\beta \leq 5.9$ the ratio of renormalization constants drops compared to the behavior at $\beta \geq 6.0$ such that the assumptions and results of the matching analysis for the D_{44} propagator must be considered with caution.

We mention that for the $SU(2)$ transversal gluon propagator it has been argued [32] that the correct instantaneous propagator can be reconstructed only from the full 4-dimensional space-time propagator. There, a residual gauge-fixing was applied that enforces $A_4 = \text{const}$. Therefore, it needs to be scrutinized whether the scaling violations, that we have seen here for the transversal gluon propagator, are really due to the alleged (multiplicative) nonrenormalizability of the Coulomb gauge [55] when residual gauge fixing is applied or not. Our results for the transversal propagator suggest a more mundane resolution: exclude too large momenta from the analysis and allow for an independently determined running lattice spacing, then data within a very restricted range of momenta (in units a) can be successfully merged and gives a $a(\beta)$ dependence that agrees with what is known from the literature.

We stress again that our result for the time-time gluon propagator is nonacceptable. The $a(\beta)$ dependence as found for this is far from the running scale for the other propagators. In the light of this, the argument of nonrenormalizability might still be valid for the A_4 component of the gluon field.

When applying fits to the data at either low or large momenta (though restricted by quite stringent bounds) we obtain qualitatively similar UV and IR fits as reported for the $SU(2)$ theory in [29].

ACKNOWLEDGMENTS

Simulations were performed on a SX-8R (NEC) vector-parallel computer at the RCNP of Osaka University and on an IBM p690 system at HLRN, Berlin and Hannover, Germany. We appreciate the warm hospitality and support of the RCNP and HLRN administrators. We thank Hinnerk Stueben for contributing parts of the code used at HLRN and help for performing simulations there. This work is partly supported by Grants-in-Aid for Scientific Research from Monbu-Kagaku-sho (No. 17340080 and 20340055). Y. N. is supported by a Grant-in-Aidfrom the Ministry of Education, Culture, Sports, Science, and Technology of Japan, and A. S. by the Australian Research Council. The work of E.-M. I. was supported by DFG through the Forschergruppe "Gitter-Hadron-Ph\"anomenologie" (FOR 465) under Contract No. Mu932/2. He is grateful to the Karl-Franzens-Universität Graz for their hospitality while this paper was being completed. E.-M. I., M. M.-P., and Y. N. gratefully acknowledge useful discussions with G. Burgio and P. Watson.

APPENDIX A: MATCHING PROCEDURE

In this appendix we describe the matching procedure of [52] applied to the Coulomb gauge. The procedure does not rely on any given lattice scale dependence $a(\beta)$ but allows us to extract this for each propagator individually.

Under the assumption that the fixed-time gluon and ghost propagators in the Coulomb gauge can be renormalized multiplicatively (see Sect. III and Ref. [50]), we aim at an optimal overlap of bare propagator data from a coarse lattice (with unknown lattice spacing a_c) and a fine lattice (with a lattice spacing a_f that might be known). Using the fact that the bare and dimensionless lattice propagator D^L is a function of the product of the three momentum p with the lattice spacing a only (the dependence on β is of course kept in mind), and assuming that multiplicative renormalization is valid, the bare propagators on the fine and coarse lattice are related by

$$a_f D_f^L(pa_f) = R_Z(a_f/a_c) \cdot a_c D_c^L(pa_c). \tag{A1}$$

The renormalization factor R_Z only depends on the ratio of the lattice cutoffs $R_a = a_f/a_c$. Taking the logarithm gives

$$\ln D_f^L(pa_f) = \ln D_c^L(pa_c) - \ln R_a + \ln R_Z. \tag{A2}$$

Expressing the momentum on the coarse lattice in terms of the momentum on the fine lattice by

$$a_c = \frac{a_f}{R_a} \quad \Longleftrightarrow \quad \ln(pa_c) = \ln(pa_f) - \ln R_a, \tag{A3}$$

we arrive at

$$\begin{aligned} \ln D_f^L[\ln(pa_f)] &= \ln D_c^L[\ln(pa_f) - \ln R_a] - \ln R_a + \ln R_Z \\ &= \ln D_c^L[\ln(pa_f) + \Delta_a] + \Delta_Z, \end{aligned} \tag{A4}$$

where $R_a = e^{-\Delta_a}$ and $R_Z = e^{-\Delta_a + \Delta_Z}$.

Notice that Δ_a and Δ_Z are positive. We find the values for R_a and R_Z from a fitting procedure as follows.

Suppose that we have one data set $\{x = pa_f, D_f^L, \sigma_f\}_i$ with $i = 1, \ldots, n_f$ for the fine lattice and one data set $\{y = pa_c, D_c^L, \sigma_c\}_j$ with $j = 1, \ldots, n_c$ for the coarse lattice with σ denoting the statistical error of the propagator D^L, with n_f and n_c denoting the number of data points for the propagator on the fine and coarse lattice, respectively. Then, we use a χ^2 fit to optimally match both data sets,

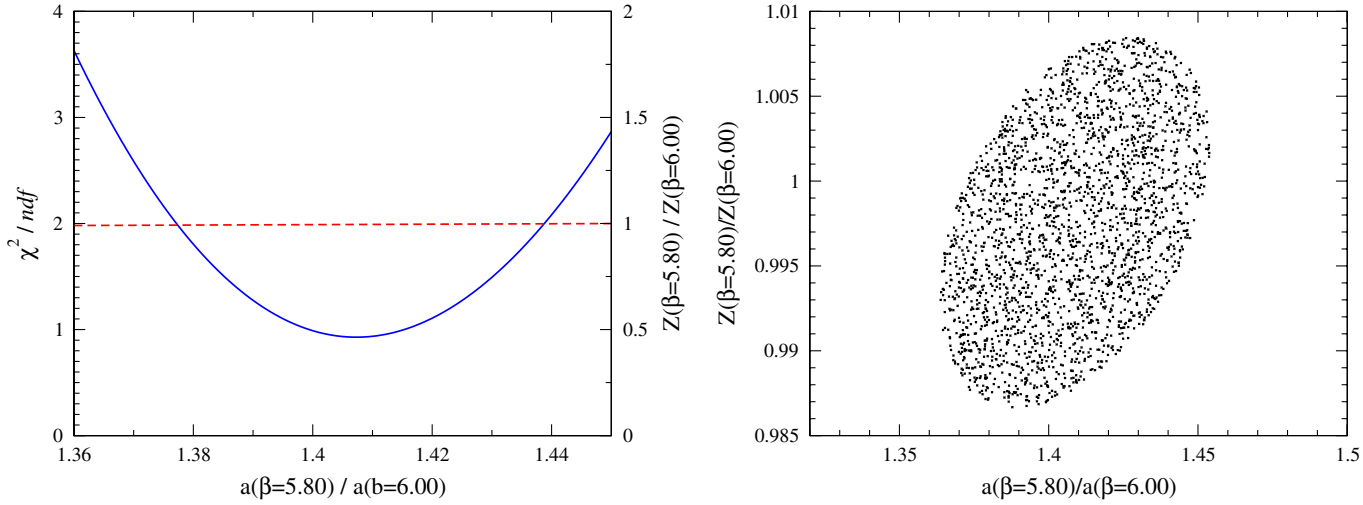

FIG. 13 (color online). Details of matching Z^{tr} measured on a $L^4 = 32^4$, $\beta = 5.8$ lattice with the data obtained on a $L^4 = 48^4$, $\beta = 6.0$ lattice. An α cut with $|p_i a| \leq 0.5$ was applied before matching. Left: χ^2/dof as a function of the ratio of lattice spacings $R_a = a_c(5.8)/a_f(6.0)$. Right: the 68.3% confidence region spanned by ratios of lattice spacing $R_a = a_c(5.8)/a_f(6.0)$ and renormalization constants $R_Z = Z(5.8)/Z(6.0)$ determined through the matching procedure.

i.e., to find the optimal overlap of the bare lattice propagator from the fine and the coarse lattice. To be specific, we minimize

$$\chi^2 = \sum_{i=1}^{n_f} \left(\frac{D_f^L(x_i) - \frac{R_Z}{R_a} D_{\mathrm{c}}^{L\ \mathrm{int}}(\frac{x_i}{R_a})}{\sigma_{f,i}} \right)^2 + \sum_{j=1}^{n_c} \left(\frac{D_c^L(y_j) - \frac{R_a}{R_Z} D_f^{L\ \mathrm{int}}(y_j R_a)}{\sigma_{c,j}} \right)^2. \quad \text{(A5)}$$

In the first term D_f^L is represented by the measured values at the momenta p_i (expressed as function of $x_i = p_i a_f$) and the corresponding error $\sigma_{f,i}$, while $D_{\mathrm{c}}^{L\ \mathrm{int}}$ is evaluated at these momenta by a cubic spline interpolation of the data for D_c^L. In the second term, the role of D_f^L and D_{c_L} is interchanged with respect to genuine data ($y_j = p_j a_c$ in D_{c_L}) and the interpolation of D_f^L. With this definition of χ^2 the matching is done as follows:

(1) Vary Δ_a over an interval (0, 1] with step size 0.001 and determine the optimal Δ_Z giving the lowest χ^2/dof for each value of Δ_a considered.
(2) Identify the best overall combination of Δ_a and Δ_Z by searching for the global minimum of χ^2/dof.

This provides us with the optimal choice of R_a and R_Z. The errors of R_a and R_Z are given by the 68.3% confidence region, i.e., the region of fit parameters R_a and R_Z with $\chi^2/\mathrm{dof} < \chi^2_{\mathrm{min}}/\mathrm{dof} + 1$. An illustration of this is given in Fig. 13 for matching the instantaneous transversal gluon propagator measured on a $L^4 = 32^4$, $\beta = 5.8$ lattice with data obtained on a $L^4 = 48^4$, $\beta = 6.0$ lattice (cf. Sec. V, Fig. 6, and Table II).

Note that applying this procedure to several combinations of fine and coarse lattices provides us with an optimal scaling relation $a = a(\beta)$ for each propagator.

TABLE I. Lattice parameters used in this study. Configurations were generated at RCNP Osaka and HU Berlin.

L^4	β	a^{-1} [GeV]	a [fm]	V [fm^4]	#conf	Group
12^4	5.8	1.446	0.1364	1.64^4	100	Berlin
16^4	...	...	...	2.18^4	40	Berlin
18^4	...	...	...	2.46^4	80	Osaka
24^4	...	...	...	3.27^4	40	Osaka
24^4	...	...	...	3.27^4	30	Berlin
32^4	...	...	...	4.36^4	20	Osaka
32^4	...	...	...	4.36^4	30	Berlin
48^4	...	...	...	6.55^4	20	Berlin
18^4	5.9	1.767	0.1116	2.09^4	80	Osaka
24^4	...	...	...	2.78^4	40	Osaka
32^4	...	...	...	3.71^4	20	Osaka
12^4	6.0	2.118	0.0932	1.12^4	100	Berlin
16^4	...	...	...	1.49^4	60	Berlin
18^4	...	...	...	1.68^4	80	Osaka
24^4	...	...	...	2.24^4	40	Osaka
24^4	...	...	...	2.24^4	40	Berlin
32^4	...	...	...	2.98^4	20	Osaka
32^4	...	...	...	2.98^4	30	Berlin
48^4	...	...	...	4.48^4	20	Berlin
18^4	6.1	2.501	0.0788	1.42^4	80	Osaka
24^4	...	...	...	1.89^4	40	Osaka
32^4	...	...	...	2.52^4	20	Osaka
12^4	6.2	2.914	0.0677	0.81^4	100	Berlin
16^4	...	...	...	1.08^4	40	Berlin
24^4	...	...	...	1.62^4	30	Berlin
32^4	...	...	...	2.17^4	20	Berlin

APPENDIX B: TABLES

In this appendix we present an overview of the data sets produced in Osaka and Berlin, the results of all matching fits according to Sec. V, VI, and VII and Appendix A as well as of the fits in the infrared (IR) and ultraviolet (UV) limits as described in Sec. IX.

TABLE II. Fit parameters obtained upon matching D^{tr} data from a $(L^4, \beta) = (32^4, 5.8)$ and a $(48^4, 6.0)$ lattice for two different α cuts (see Fig. 6). For comparison we also show the lattice-spacing ratios according to Eq. (18).

$\lvert p_i a\rvert \leq \alpha$	$\frac{a(5.8)}{a(6.0)}$	$\frac{a^{\mathrm{NS}}(5.8)}{a^{\mathrm{NS}}(6.0)}$	$R_Z(\frac{a(5.8)}{a(6.0)})$	χ^2/dof
$\alpha = 0.6$	1.37^{+3}_{-4}	1.46	0.989^{+10}_{-10}	3.28
$\alpha = 0.5$	1.41^{+4}_{-5}	1.46	0.998^{+11}_{-11}	0.92

TABLE III. Matching the transversal gluon propagator for five β values (see Fig. 7): shown are the ratios of lattice spacings relative to the finest one obtained either by the matching procedure or according to Eq. (18); the ratios of the renormalization constants and the corresponding χ^2/dof of the fit that accomplishes the matching for four choices of the α cut. The lattice size is 32^4.

$\lvert p_i a\rvert \leq \alpha$	β	$\frac{a(\beta)}{a(6.2)}$	$\frac{a^{\mathrm{NS}}(\beta)}{a^{\mathrm{NS}}(6.2)}$	$R_Z(\frac{a(\beta)}{a(6.2)})$	χ^2/dof
$\alpha = 1.0$	5.8	1.51^{+4}_{-4}	2.01	0.982^{+12}_{-13}	5.56
	5.9	1.31^{+5}_{-5}	1.65	0.990^{+19}_{-18}	3.83
	6.0	1.19^{+7}_{-7}	1.38	0.993^{+34}_{-26}	2.39
	6.1	1.12^{+10}_{-20}	1.17	0.984^{+108}_{-36}	6.30
$\alpha = 0.8$	5.8	1.68^{+4}_{-6}	2.01	0.961^{+12}_{-10}	2.16
	5.9	1.43^{+5}_{-6}	1.65	0.970^{+16}_{-15}	2.98
	6.0	1.27^{+7}_{-9}	1.38	0.973^{+35}_{-23}	2.61
	6.1	1.18^{+8}_{-13}	1.17	0.968^{+52}_{-25}	5.26
$\alpha = 0.6$	5.8	1.74^{+5}_{-5}	2.01	0.974^{+9}_{-9}	1.41
	5.9	1.46^{+4}_{-5}	1.65	0.980^{+12}_{-11}	1.70
	6.0	1.28^{+9}_{-7}	1.38	0.983^{+23}_{-22}	2.97
	6.1	1.18^{+9}_{-7}	1.17	0.976^{+27}_{-27}	1.87
$\alpha = 0.5$	5.8	1.92^{+7}_{-6}	2.01	0.963^{+8}_{-8}	0.585
	5.9	1.58^{+5}_{-4}	1.65	0.967^{+9}_{-9}	2.49
	6.0	1.39^{+9}_{-9}	1.38	0.970^{+19}_{-19}	1.96
	6.1	1.23^{+12}_{-9}	1.17	0.968^{+27}_{-26}	1.59

TABLE IV. Fit parameters obtained upon matching the instantaneous time-time gluon propagator on a $L^4 = 32^4$, $\beta = 5.8$ and a $L^4 = 48^4$, $\beta = 6.0$ lattice with two different α cuts (see Fig. 8). For comparison we show also the lattice-spacing ratio predicted by the Necco-Sommer scaling relation.

$\lvert p_i a\rvert \leq \alpha$	$\frac{a(5.8)}{a(6.0)}$	$\frac{a^{\mathrm{NS}}(5.8)}{a^{\mathrm{NS}}(6.0)}$	$R_Z(\frac{a(5.8)}{a(6.0)})$	χ^2/dof
$\alpha = 0.6$	1.96^{+17}_{-9}	1.46	0.476^{+48}_{-55}	4.50
$\alpha = 0.5$	1.87^{+12}_{-10}	1.46	0.502^{+42}_{-40}	0.503

TABLE V. Matching the time-time gluon propagator for four β values on 32^4 lattices (Osaka data): shown are the ratios of the lattice spacings obtained by the matching relative to the finest one, for comparison the ratios predicted by Necco-Sommer scaling are also included; the ratios of the renormalization constants and the corresponding χ^2/dof of the fit that accomplishes the matching, for two choices of the α cut.

$\lvert p_i a\rvert \leq \alpha$	β	$\frac{a(\beta)}{a(6.1)}$	$\frac{a^{\mathrm{NS}}(\beta)}{a^{\mathrm{NS}}(6.1)}$	$R_Z(\frac{a(\beta)}{a(6.1)})$	χ^2/dof
$\alpha = 0.6$	5.8	2.72^{+64}_{-10}	1.73	0.327^{+19}_{-84}	4.94
	5.9	2.04^{+49}_{-13}	1.42	0.429^{+44}_{-128}	13.9
	6.0	1.07^{+6}_{-4}	1.18	1.04^{+7}_{-7}	8.70
$\alpha = 0.5$	5.8	2.60^{+18}_{-26}	1.73	0.350^{+53}_{-32}	1.45
	5.9	1.81^{+5}_{-18}	1.42	0.509^{+96}_{-29}	1.03
	6.0	1.08^{+8}_{-8}	1.18	1.03^{+15}_{-12}	6.19

TABLE VI. Matching the time-time gluon propagator for three β values on 32^4 lattices (Berlin data): shown are the ratios of lattice spacings obtained by the matching relative to the finest one, for comparison the ratios predicted by Necco-Sommer scaling are also included; the ratios of the renormalization constants and the corresponding χ^2/dof of the fit that accomplishes the matching for two choices of the α cut.

$\lvert p_i a\rvert \leq \alpha$	β	$\frac{a(\beta)}{a(6.2)}$	$\frac{a^{\mathrm{NS}}(\beta)}{a^{\mathrm{NS}}(6.2)}$	$R_Z(\frac{a(\beta)}{a(6.2)})$	χ^2/dof
$\alpha = 0.6$	5.8	2.61^{+0}_{-12}	2.01	0.292^{+24}_{-4}	15.7
	6.0	1.11^{+5}_{-4}	1.38	0.996^{+57}_{-76}	3.98
$\alpha = 0.5$	5.8	1.89^{+0}_{-7}	2.01	0.487^{+38}_{-5}	11.0
	6.0	1.09^{+7}_{-6}	1.38	1.02^{+11}_{-10}	5.56

TABLE VII. Matching the ghost propagator for four β values on 32^4 lattices (Osaka data): shown are ratios of lattice spacings obtained by the matching relative to the finest one, for comparison the ratios predicted by Necco-Sommer scaling are also included; the ratios of the renormalization constants, and the corresponding χ^2/dof of the fit that accomplishes the matching, without α cut ($\alpha = 2.0$) and for two choices of the α cut.

$\lvert p_i a\rvert \leq \alpha$	β	$\frac{a(\beta)}{a(6.1)}$	$\frac{a^{\mathrm{NS}}(\beta)}{a^{\mathrm{NS}}(6.1)}$	$R_Z(\frac{a(\beta)}{a(6.1)})$	χ^2/dof
$\alpha = 2.0$	5.8	1.67^{+2}_{-2}	1.73	0.955^{+2}_{-3}	1.63
	5.9	1.39^{+2}_{-3}	1.42	0.971^{+3}_{-2}	0.840
	6.0	1.18^{+1}_{-2}	1.18	0.985^{+2}_{-1}	0.260
$\alpha = 0.6$	5.8	1.48^{+17}_{-11}	1.73	0.998^{+31}_{-44}	0.219
	5.9	1.34^{+9}_{-8}	1.42	0.981^{+23}_{-28}	0.583
	6.0	1.17^{+6}_{-6}	1.18	0.987^{+17}_{-17}	0.420
$\alpha = 0.5$	5.8	1.43^{+22}_{-21}	1.73	1.02^{+9}_{-7}	0.268
	5.9	1.35^{+17}_{-17}	1.42	0.979^{+61}_{-50}	0.854
	6.0	1.18^{+10}_{-8}	1.18	0.982^{+31}_{-29}	0.501

TABLE VIII. Matching the ghost propagator for three β values on 32^4 lattices (Berlin data): shown are ratios of the lattice spacings obtained by the matching relative to the finest one, for comparison the ratios predicted by Necco-Sommer scaling are also included; the ratios of the renormalization constants and the corresponding χ^2/dof of the fit that accomplishes the matching, without α cut ($\alpha = 2.0$) and for two choices of the α cut.

$\lvert p_i a\rvert \le \alpha$	β	$\frac{a(\beta)}{a(6.2)}$	$\frac{a^{\mathrm{NS}}(\beta)}{a^{\mathrm{NS}}(6.2)}$	$R_Z(\frac{a(\beta)}{a(6.2)})$	χ^2/dof
$\alpha = 2.0$	5.8	1.91^{+1}_{-1}	2.01	0.944^{+1}_{-1}	10.4
	6.0	1.34^{+1}_{-1}	1.38	0.976^{+1}_{-1}	54.6
$\alpha = 0.6$	5.8	1.80^{+1}_{-0}	2.01	0.959^{+1}_{-3}	38.5
	6.0	1.27^{+1}_{-1}	1.38	0.987^{+3}_{-2}	121
$\alpha = 0.5$	5.8	1.40^{+3}_{-3}	2.01	1.08^{+1}_{-1}	18.5
	6.0	1.18^{+2}_{-1}	1.38	1.02^{+1}_{-1}	19.3

TABLE IX. Fitted UV parameters and χ^2/dof for the transverse gluon propagator. Data from RCNP, Osaka. $a = a(\beta = 6.2) = 0.1354 r_0$.

$\lvert p_i a\rvert \le \alpha$	$[pa]_{\mathrm{min}}$	$c_{\mathrm{tr}} a$	η_{tr}	χ^2/dof
$\alpha = 0.5$	0.5	0.507(5)	0.39(2)	0.50
	0.6	0.518(20)	0.42(6)	0.98
$\alpha = 0.6$	0.5	0.534(5)	0.46(1)	0.81
	0.6	0.537(6)	0.46(2)	0.70
	0.7	0.517(15)	0.43(3)	0.75
	0.8	0.489(50)	0.39(6)	1.55

TABLE X. Fitted UV parameters and χ^2/dof for the time-time dressing function Z_{44} with an α cut for $\alpha = 0.5$. $a = a(\beta = 6.0) = 0.1863 r_0$.

data	$[pa]_{\mathrm{min}}$	$c_{44} a$	η_{44}	χ^2/dof
Osaka	0.65	0.942(8)	2.53(10)	1.75
	0.60	0.946(6)	2.47(6)	1.19
	0.55	0.945(4)	2.48(4)	0.81
	0.50	0.940(4)	2.54(3)	2.18
Berlin	0.79	0.968(16)	2.09(22)	0.23
	0.75	0.962(10)	2.19(11)	0.26
	0.70	0.962(9)	2.19(10)	0.18
	0.65	0.948(5)	2.38(5)	1.16
	0.60	0.940(4)	2.49(4)	2.22

TABLE XI. Fitted IR parameters and χ^2/dof for the time-time dressing function Z_{44} with an α cut for $\alpha = 0.5$. $a = a(\beta = 6.0) = 0.1863 r_0$.

data	$[pa]_{\mathrm{max}}$	$d_{44} a$	κ_{44}	χ^2/dof
Osaka	0.20	2.07(14)	1.71(5)	0.057
	0.25	1.52(4)	1.94(3)	19.5
	0.30	1.36(3)	2.05(2)	20.3
Berlin	0.20	4.25(32)	1.26(3)	18.2
	0.25	2.75(8)	1.44(2)	21.2
	0.30	2.16(4)	1.57(1)	47.0

TABLE XII. Fitted UV parameters and χ^2/dof for the ghost dressing function [$a = a(\beta = 6.0) = 0.1863 r_0$].

$\lvert p_i a\rvert \le \alpha$	$[pa]_{\mathrm{min}}$	c_{gh}	$\Lambda_{\mathrm{Coul}} a$	γ	χ^2/dof
$\alpha = 0.5$	0.70	1.39(1)	0.52(27)	0.13(19)	0.52
	0.75	1.62(91)	0.26(38)	0.38(53)	0.91
$\alpha = 0.6$	0.85	1.58(6)	0.277(28)	0.365(28)	3.88
	0.9	1.44(9)	0.370(81)	0.289(58)	2.81
$\alpha = 2.0$	2.0	1.50(1)	0.313(2)	0.313(1)	3.96
	2.5	1.51(1)	0.300(5)	0.319(2)	2.61
	3.0	1.56(2)	0.274(12)	0.329(6)	1.53
	3.5	1.55(4)	0.273(31)	0.330(14)	1.18
	4.0	1.55(3)	0.270(23)	0.332(10)	0.87

TABLE XIII. Fitted IR parameters and χ^2/dof for the ghost dressing function [$a = a(\beta = 6.0) = 0.1863 r_0$].

$\lvert p_i a\rvert \le \alpha$	$[pa]_{\mathrm{max}}$	$d_{\mathrm{gh}} a$	κ_{gh}	χ^2/dof
$\alpha = 0.5$	0.29	2.48(10)	0.439(7)	10.9
	0.30	2.45(9)	0.442(7)	8.55
	0.34	2.19(5)	0.463(5)	8.20
$\alpha = 0.6$	0.25	2.57(10)	0.435(6)	0.62
	0.27	2.54(9)	0.437(6)	3.79
	0.30	2.50(9)	0.440(6)	4.32
$\alpha = 2.0$	0.24	2.57(9)	0.434(6)	5.64
	0.30	2.52(9)	0.437(6)	5.90

[1] J. E. Mandula and M. Ogilvie, Phys. Lett. B **185**, 127 (1987).
[2] P. Marenzoni, G. Martinelli, and N. Stella, Nucl. Phys. **B455**, 339 (1995).
[3] H. Suman and K. Schilling, Phys. Lett. B **373**, 314 (1996).
[4] A. Nakamura, H. Aiso, M. Fukuda, T. Iwamiya, T. Nakamura, and M. Yoshida, arXiv:hep-lat/9506024.
[5] D. B. Leinweber, J. I. Skullerud, A. G. Williams, and C. Parrinello, Phys. Rev. D **58**, 031501(R) (1998).
[6] D. Becirevic *et al.*, Phys. Rev. D **60**, 094509 (1999).
[7] J. E. Mandula, Phys. Rep. **315**, 273 (1999).
[8] L. von Smekal, A. Hauck, and R. Alkofer, Phys. Rev. Lett. **79**, 3591 (1997).
[9] L. von Smekal, A. Hauck, and R. Alkofer, Ann. Phys. (N.Y.) **267**, 1 (1998).
[10] F. D. R. Bonnet, P. O. Bowman, D. B. Leinweber, and A. G. Williams, Phys. Rev. D **62**, 051501(R) (2000).
[11] F. D. R. Bonnet, P. O. Bowman, D. B. Leinweber, A. G. Williams, and J. M. Zanotti, Phys. Rev. D **64**, 034501 (2001).

[12] P. O. Bowman, U. M. Heller, D. B. Leinweber, M. B. Parappilly, and A. G. Williams, Phys. Rev. D **70**, 034509 (2004).
[13] A. Sternbeck, E.-M. Ilgenfritz, M. Müller-Preussker, and A. Schiller, Phys. Rev. D **72**, 014507 (2005).
[14] E.-M. Ilgenfritz, M. Müller-Preussker, A. Sternbeck, A. Schiller, and I. L. Bogolubsky, Braz. J. Phys. **37**, 193 (2007).
[15] A. Sternbeck, E.-M. Ilgenfritz, M. Müller-Preussker, A. Schiller, and I. L. Bogolubsky, Proc. Sci., LAT2006 (2006) 076.
[16] A. Sternbeck, L. von Smekal, D. B. Leinweber, and A. G. Williams, Proc. Sci., LAT2007 (2007) 340.
[17] I. L. Bogolubsky, E.-M. Ilgenfritz, M. Müller-Preussker, and A. Sternbeck, Proc. Sci., LAT2007 (2007) 290.
[18] P. O. Bowman *et al.*, Phys. Rev. D **76**, 094505 (2007).
[19] W. Kamleh, P. O. Bowman, D. B. Leinweber, A. G. Williams, and J. Zhang, Phys. Rev. D **76**, 094501 (2007).
[20] A. Cucchieri and T. Mendes, Proc. Sci., LAT2007 (2007) 297.
[21] I. L. Bogolubsky, E. M. Ilgenfritz, M. Müller-Preussker, and A. Sternbeck, Phys. Lett. B **676**, 69 (2009).
[22] C. Lerche and L. von Smekal, Phys. Rev. D **65**, 125006 (2002).
[23] D. Zwanziger, Phys. Rev. D **65**, 094039 (2002).
[24] J. M. Pawlowski, D. F. Litim, S. Nedelko, and L. von Smekal, Phys. Rev. Lett. **93**, 152002 (2004).
[25] C. S. Fischer and J. M. Pawlowski, Phys. Rev. D **75**, 025012 (2007).
[26] C. S. Fischer, A. Maas, and J. M. Pawlowski, arXiv:0810.1987.
[27] A. Sternbeck and L. von Smekal, arXiv:0811.4300.
[28] C. S. Fischer and J. M. Pawlowski, arXiv:0903.2193.
[29] K. Langfeld and L. Moyaerts, Phys. Rev. D **70**, 074507 (2004).
[30] A. Cucchieri and D. Zwanziger, Phys. Rev. D **65**, 014001 (2001).
[31] M. Quandt, G. Burgio, S. Chimchinda, and H. Reinhardt, Proc. Sci., LAT2007 (2007) 325.
[32] G. Burgio, M. Quandt, and H. Reinhardt, Phys. Rev. Lett. **102**, 032002 (2009).
[33] H. Reinhardt and C. Feuchter, Phys. Rev. D **71**, 105002 (2005).
[34] W. Schleifenbaum, M. Leder, and H. Reinhardt, Phys. Rev. D **73**, 125019 (2006).
[35] D. Epple, H. Reinhardt, and W. Schleifenbaum, Phys. Rev. D **75**, 045011 (2007).
[36] D. Epple, H. Reinhardt, W. Schleifenbaum, and A. P. Szczepaniak, Phys. Rev. D **77**, 085007 (2008).
[37] Y. Nakagawa, H. Toki, A. Nakamura, and T. Saito, Proc. Sci., LAT2007 (2007) 319.
[38] D. Zwanziger, Nucl. Phys. **B518**, 237 (1998).
[39] D. Zwanziger, Phys. Rev. Lett. **90**, 102001 (2003).
[40] Y. Nakagawa, A. Nakamura, T. Saito, H. Toki, and D. Zwanziger, Phys. Rev. D **73**, 094504 (2006).
[41] Y. Nakagawa, A. Nakamura, T. Saito, and H. Toki, Phys. Rev. D **77**, 034015 (2008).
[42] J. Greensite, S. Olejnik, and D. Zwanziger, J. High Energy Phys. 05 (2005) 070.
[43] Y. Nakagawa, A. Nakamura, T. Saito, and H. Toki, Phys. Rev. D **75**, 014508 (2007).
[44] A. Voigt, E.-M. Ilgenfritz, M. Müller-Preussker, and A. Sternbeck, Proc. Sci., LAT2007 (2007) 338.
[45] A. Voigt, E.-M. Ilgenfritz, M. Müller-Preussker, and A. Sternbeck, Phys. Rev. D **78**, 014501 (2008).
[46] D. Zwanziger, Phys. Rev. D **70**, 094034 (2004).
[47] V. N. Gribov, Nucl. Phys. **B139**, 1 (1978).
[48] D. Zwanziger, Nucl. Phys. **B364**, 127 (1991).
[49] T. Kugo and I. Ojima, Prog. Theor. Phys. Suppl. **66**, 1 (1979).
[50] P. Watson and H. Reinhardt, Phys. Rev. D **77**, 025030 (2008).
[51] S. Necco and R. Sommer, Nucl. Phys. **B622**, 328 (2002).
[52] D. B. Leinweber, J. I. Skullerud, A. G. Williams, and C. Parrinello, Phys. Rev. D **60**, 094507 (1999).
[53] P. Boucaud *et al.*, Phys. Rev. D **72**, 114503 (2005).
[54] F. de Soto and C. Roiesnel, J. High Energy Phys. 09 (2007) 007.
[55] P. Watson and H. Reinhardt, Phys. Rev. D **76**, 125016 (2007).